32.0 DEVELOPMENT OF CABINET BASED COMPUTED TOMOGRAPHY METHODS FOR STUDIES OF MICROSTRUCTURES AND DEFECTS IN METALS (LEVERAGED)

C. Gus Becker (Mines)
Faculty: Amy Clarke (Mines)
Industrial Mentor: Michelle Espy (LANL)

This project initiated in Fall 2017 and is supported directly by Los Alamos National Laboratory (LANL). The research performed during this project will serve as the basis for a Ph.D. thesis program for C. Gus Becker.

32.1 Project Overview and Industrial Relevance

X-ray radiography allows for the imaging of materials in a non-destructive manner by observing the x-rays transmitted through the material. It can be used for post-mortem analysis, as well as in-situ imaging capable of capturing the development of microstructure during processing. This is important in the study of solidification, for example. Dynamic imaging of microstructure evolution during processing (e.g. casting or directional solidifcation) can further our understanding of the mechanisms driving microstructural development, leading to improved predictive capabilities [32.1]. X-ray radiography can also be used to capture multiple images of a sample from different angles that can be reconstructed and combined into a three-dimensional representation. For instance, a reconconstruction of an additively manufactured (AM) metal sample can be generated to reveal internal defects in the part. Four-dimensional microscopy (three spatial and one temporal dimension), in which images are collected from different angles of a sample that is evolving in time, can also be performed to create an evolving, three-dimensional reconstruction. These reconstructions are created using techniques like Time-Interlaced Model-Based Iterative Reconstruction (TIMBIR) [32.2], which improves temporal resolution to capture microstructural evolution during processing.

Synchrotron x-ray sources can be used to obtain high-spatial resolution x-ray radiographs (on the order of 1 µm), however these images have a small field of view and require significant beam time at an often oversubscribed national user facility. High-energy micro-focus x-ray radiography has a drawback of lower spatial resolutions, but increases the field of view significantly and can be performed in a laboratory. These laboratory instruments consist of a high-energy micro-focus x-ray source, radiation shielding typically in the form of a lead-lined cabinet inside of which the source is located, a scintillator to convert x-rays to visible light, and a detector to collect that light. Tomographic data can be obtained when a rotation stage for the sample is included.

Solidifiation experiments are often performed at synchrotron x-ray facilities like the Advanced Photon Source (APS) at Argonne National Laboratory, as well as in facilities with micro-focus x-rays capabilities like Los Alamos National Laboratory (LANL) to study the microstructures and properties of materials. Many of these experiments have been performed by our group to study different aspects of alloy solidification, such as crystal growth and solute segregation [32.1], primary dendrite spacing and size [32.3], dendrite fragmentation [32.4], and the effect of cooling rates [32.5].

When x-ray radiography and computed tomography are used for the non-destructive imaging of metals, high densities may constrain experiments by sample thickness. X-rays at national user facilities can typically penetrate thin foils of material (~100 µm to ~1 mm) to image thin sections or small volumes to produce computed tomographic reconstructions utilizing x-rays with energies of around 30 keV [32.5], but typically cannot be used to image larger samples, unless special high-energy beamlines are used with x-ray energies up to ~150 keV. High-energy micro-focus x-ray imaging utilizes x-rays with energies of up to 250 keV, for example, allowing sample thicknesses on the order of millimeters and significantly larger fields-of-view. Proton radiography (pRad), in which 800 MeV energy protons are transmitted through samples at LANL's Los Alamos Neutron Science Center (LANSCE), allows for even larger sample sizes and the ability to probe materials with high atomic numbers at the cost of somewhat lower spatial resolution [32.1]. There have also been proof-of-concept experiments of Transmission High-Energy Electron Microscopy (THEEM), in which extremely high-energy electrons (15 GeV) are transmitted through samples at the Stanford Linear Accelerator Center (SLAC) to achieve deeply penetrating electron radiography [32.6]. This method has yet to be optimized, but holds potential for high-Z materials.

32.2 Previous Work

Prior to the start of this project, in-situ solidification studies were performed at the APS using synchrotron x-ray imaging and in a laboratory setting, in collaboration with the Non-Destructive Testing group at LANL (E-6, formerly

AET-6) using high-energy micro-focus x-ray radiography. An image processing method has been created to process the data from these and other experiments. Once processed, this data can be analyzed to capture the multi-scale solidification dynamics in metallic alloys. One of the goals of this project is to establish a high-energy micro-focus x-ray cabinet at Mines for metallic alloy investigation to further the study of solidification and additive maufacturing (AM) related defects.

This initial image processing method, created using the script editor within ImageJ, consists of modular image processing scripts. Each script takes a directory of images from an experiment and performs a programmed process to enhance the images in some way, saving the results as separate files to preserve the original, unedited images. The modular nature of these scripts allows for the processing steps to be reperformed in different sequences on the original images, adding to or changing the image processing steps to achieve different results. This method is presented by processing a high-energy micro-focus solidification experiment performed with E-6 using the same set up as previous synchrotron x-ray experiments. This set up consists of a steel bar with a rectangular window cut into it to aid in the transmittance of x-rays. Micro-focus x-ray radiography allows for a larger field of view than synchrotron x-ray radiography, so the experiment designed for synchrotron radiography takes place in only a fraction of the entire captured image, as seen in the directional solidification of an Al-Ag alloy in **Figure 32.1a**. This experiment will be used to demonstrate the current processing abilities of the modular image processing method. The first script extracts the lighter portion of the radiographs from these experiments by thresholding the pixel values in the image corresponding to the lighter window, as seen in **Figure 32.1b**. Another script can remove a set amount of pixels from each side of the images, therefore allowing for better contrast within the desired subject area by removing partial features that were not completely extracted by thresholding. The result of this script can be seen in **Figure 32.2a.** While this image exhibits better contrast between the dendrites and the interdendritic regions of the solidificaiton structure, there are still artifacts from the imaging process represented as vertical and horizontal banding. This can be adjusted with a script that performs a fast Fourier transform to filter out repeated structures of the banding. The result of this script can be seen in **Figure 32.2b.**

32.3   Recent Progress

A multitude of image processing techniques are available through the use of the Python programming language and the Python package scikit-image [32.7]. Some of these techniques have been tested using Dynamic Transmission Electron Microscopy (DTEM) data obtained at Lawrenec Livermore National Laboratory (LLNL) of various compositions of solidifying Al-Ge. An example DTEM image is shown in **Figure 32.4a.** This data was chosen as a candidate for the exploration of Python for many reasons: the resemblance in the DTEM images to x-ray radiographs that are captured with high-energy micro-focus systems, the high amount of noise in the data that allow for the deployment of restoration and denoising algorithms, the juxtaposition of multiple frames in each DTEM image that requires an elaborate segmentation technique to separate individual frames, and finally as a way to clean up the DTEM data and prepare it for publication.

The first step in processing the DTEM data is to reduce the amount of noise in each image. A total variation minimazation algorithm [32.8] achieved the best results. The denoised image can be seen in **Figure 32.4b.** The next processing steps were taken to segment the image into its separate frames, allowing each frame to be extracted from the original image. This was done using a technique known as watershed segmentation, performed using functions once again from the scikit-image package. The watershed algorithm is named for a useful metaphor to understand how it works: the values of the pixels in an image are thought of as elevations, and points are chosen on the image "topography" to start filling the image with water. Typically the lowest pixel values in the image (which would correspond to the valleys in the topography metaphor) are used as the seeds to start filling the area with water, but other locations can be used as seeds as long as they are specified and properly fed into the algorithm. The water then fills up the image until it reaches a defined boundary or another water basin. The result of the algorthim is a separate region for each individual water basin.

The steps for this technique as applied to the example DTEM image are illustrated in **Figure 32.5**. An automatic minimum threshold is applied to the denoised image to produce a binary mask separating the image into two regions: a light area representing the data, and a dark area representing the background (**Figure 32.5b**). A distance map is then created that maps each pixel within the light area with a value that correlates to the distance to the nearest background area (**Figure 32.5c**). The darker the pixel, the father it is from the background. The watershed segmentation is then performed using local maxima of the distance map as the seed. The final regions obtained from the watershed

segmentation are represented by different colors in **Figure 32.5d.** Once the regions are separated, they can be extracted from the original image using the coordinates of the bouding box of each region. The extracted regions are shown in **Figure 32.6**. From the extracted regions, an animation can be produced as another way of demontrating the solidifaction of Al45Ge and the evolution of the nucleated grain.

32.4   Plans for Next Reporting Period

Although the ImageJ scripting method was used as at the beginning of this project for image processing, it is now apparent that enlisting Python as the main image processing tool will be more useful and efficient. To prepare for the installment of the high-energy micro-focus x-ray cabinet at Mines, the scripts that were written in ImageJ to handle the kind of data we can expect to obtain from the cabinet will be reevaluated to determine if they can be improved with Python. In the short term, the following tasks will be completed:

- Create an improved segmentation technique in Python to replace the script used to improve the process of extracting features from images as in **Figure 32.1b**.

- Investigate the fast Fourier transform filtering ability of Python to improve the technique of reducing banding in images as in **Figure 32.2b**.

- Quantitatively analyze microstructural features from solidification experiments in processed data (e.g. solidification velocity, pixel values corresponding to local solute variations).

- Prepare laboratory space where the micro-focus x-ray cabinet will be installed at Mines.

- Practice using TomoPy reconstruction package in Python to produce tomographic representations of samples like that seen in **Figure 32.6** with Al-Cu, Al-Ag, and Al-Cu-Ag tomography data obtained by Brian Milligan *et al.* at the APS as a way to prepare for tomography experiments with E-6 and with the new micro-focus x-ray cabinet at Mines.

- Continue working with E-6 to identify useful experiments involving static imaging of AM builds.

32.5   References

[32.1] P.J. Gibbs, S.D. Imhoff, C.L. Morris, F.E. Merrill, C.H. Wilde, P. Nedrow, F.G. Mariam, K. Fezzaa, W.-K. Lee, A.J. Clarke, Multiscale X-ray and proton imaging of Sn-Bi solidification, JOM. 66 (2014) 1485–1492.

[32.2] K. Aditya Mohan, S.V. Venkatakrishnan, J.W. Gibbs, E.B. Gulsoy, X. Xiao, M. De Graef, P.W. Voorhees, C.A. Bouman, TIMBIR: a method for time-space reconstruction from interlaced views, IEEE Trans. on Comp. Imaging. 1 (2015) 96-111.

[32.3] A.J. Clarke, D. Tourret, Y. Song, S.D. Imhoff, P.J. Gibbs, J.W. Gibbs, K. Fezzaa, A. Karma, Microstructure selection in thin-sample directional solidification of an Al-Cu alloy: in situ x-ray imaging and phase-field simulations, Acta Materialia. 129 (2017) 203-216.

[32.4] J.W. Gibbs, D. Tourret, P.J. Gibbs, S.D. Imhoff, M.J. Gibbs, B.A. Walker, K. Fezzaa, A.J. Clarke, In situ x-ray observations of dendritic fragmentation during directional solidification of a Sn-Bi alloy, JOM. 68 (2016) 170-177.

[32.5] B.M. Patterson, K.C. Henderson, P.J. Gibbs, S.D. Imhoff, A.J. Clarke, Laboratory micro- and nanoscale X-ray tomographic investigation of Al-7 at.%Cu solidification structures, Mat. Char. 95 (2014) 18-26.

[32.6] F.E. Merrill, J. Goett, J.W. Gibbs, S.D. Imhoff, F.G. Mariam, C.L. Morris, L.P. Neukirch, J. Perry, D. Poulson, R. Simpson, P.L. Volegov, P.L. Walstrom, C.H. Wilde, C. Hast, K. Jobe, T. Smith, U. Wienands, A.J. Clarke, D. Tourret, Demonstration of transmission high energy electron microscopy, App. Phys. Lett. 112 (2018) 144103.

[32.7] A. Chambolle, An Algorithm for Total Variation Minimization and Applications, Journal of Mathematical Imaging and Vision. 20 (2004) 89–97.

[32.8] S. van der Walt, J. L. Schönberger, J. Nunez-Iglesias, F. Boulogne, J. D. Warner, N. Yager, E. Gouillart, T. Yu, Scikit-Image: Image Processing in Python, PeerJ. 2 (2014) 453-471.
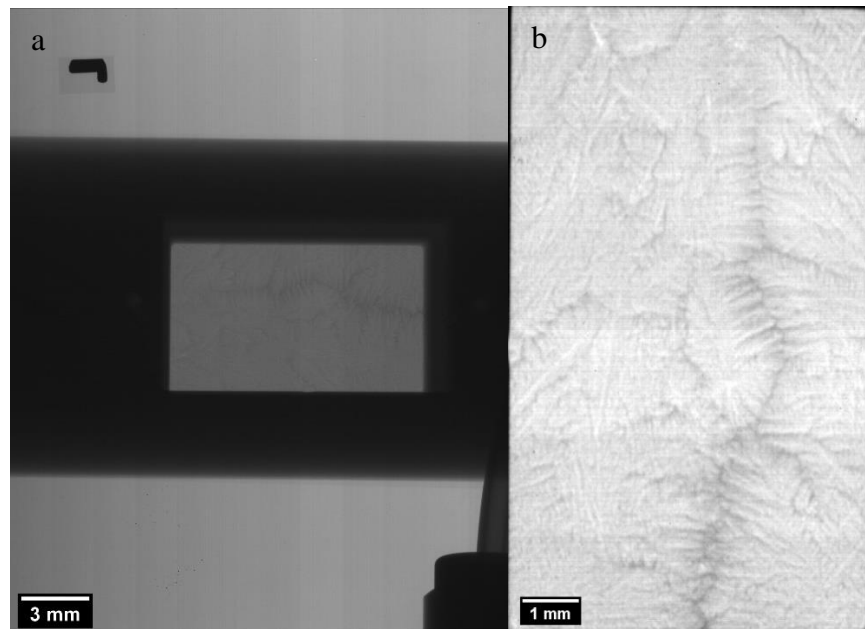
32.6 Figure and Tables

Figure 32.1: A frame from the solidification process of an Al-Ag alloy obtained using high-energy micro-focus x-ray radiography of a sample undergoing directional solidification. The experiment was performed using the synchrotron x-ray radiography setup, so the experiment is entirely contained in the small, light gray window in the center of (a) and cropped to that window in (b). Laboratory x-ray imaging affords new opportunities to study larger fields-of-view.
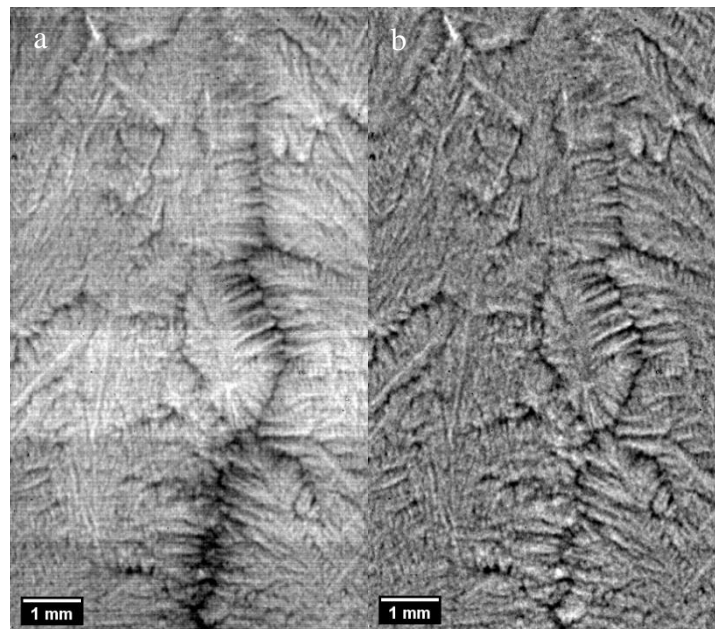

Figure 32.2: Further processing of the same frame of Al-Ag solidification shown in **Figure 32.1** by (a) trimming 10 pixels from each edge of the radiograph, allowing for better contrast in the solidification structure, and (b) performing fast Fourier transform filtering to remove horizontal and vertical banding artifacts.
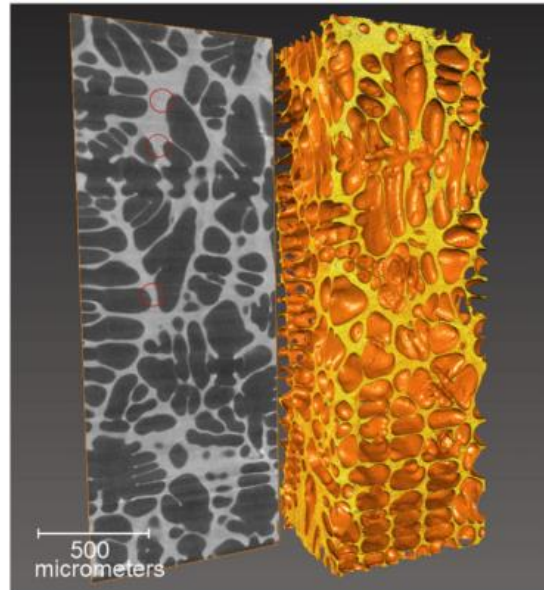
Figure 32.3: Three-dimensional tomographic reconstruction of an Al-Cu alloy from multiple radiographs. Reconstructions allow for manipulation of data unavailable from radiographs alone. The Al-rich primary dendrites in the reconstruction have been rendered translucent to better show the Cu-containing eutectic in orange [32.5].
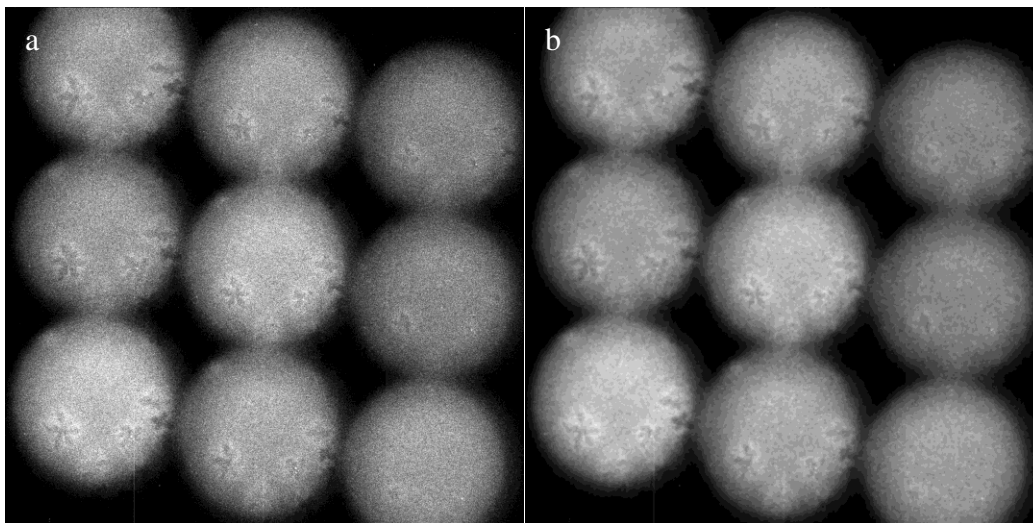

Figure 32.4: Solidification of Al45Ge represented by (a) the original DTEM image, and (b) the image when a Chambolle Total Variation Filter [32.7] is applied with a weight of 0.3. Each image contains nine frames, the chronological order of which begins in the lower right corner, moves up to the top right, left to top center, down to bottom center, left to bottom left, and finally up to top left.
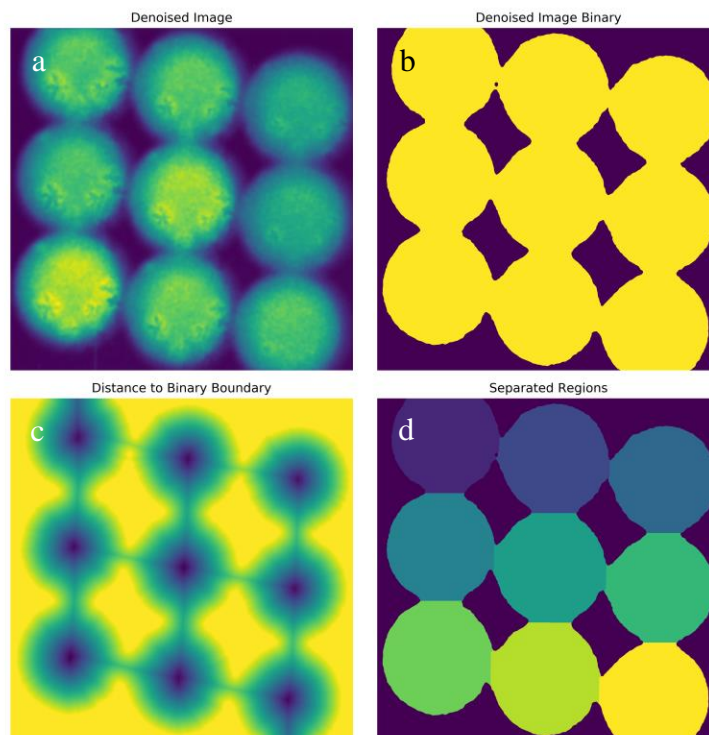
32.5

Figure 32.5: Segmentation process of (a) the denoised Al45Ge DTEM image, (b) the binary mask created using the minimum thresholding method in scikit-image, (c) the distance map created by mapping each point inside of the binary mask with a value that correlates the distance to the edge of the mask, and (d) the regions obtained by performing a watershed segmentation using the local maxima of the distance map as the seed. A purple to yellow colormap is used to more easily distinguish between pixel values.
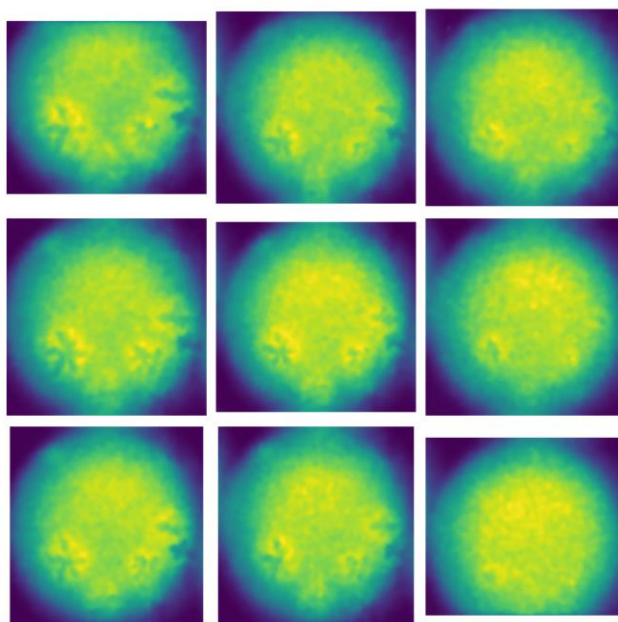

Figure 32.6: Segmented regions of the denoised Al45Ge DTEM image obtained by performing the watershed segmentation process as illustrated in **Figure 32.5**.

32.6